technologies

MDPI

Article

Study on the Dynamic Response of the Carbody–Anti-Bending Bars System

Ioana-Izabela Apostol, Traian Mazilu * and Mădălina Dumitriu *

Department of Railway Vehicles, National University of Science and Technology Politehnica Bucharest, 060042 Bucharest, Romania; ioana.apostol96@upb.ro

* Correspondence: traian.mazilu@upb.ro (T.M.); madalina.dumitriu@upb.ro (M.D.)

Abstract: Ride comfort is an important requirement that passenger rail vehicles must meet. Carbody–anti-bending system is a relatively new passive method to enhance the ride comfort in passenger rail vehicles with long and light carbody. The resonance frequency of the first bending mode (FBM) of such vehicle is within the most sensitive frequency range that affects ride comfort. Anti-bending bars consist of two bars that are mounted under the longitudinal beams of the carbody chassis using vertical supports. When the carbody bends, the anti-bending bars develop moments in the neutral axis of the carbody opposing the bending of the carbody. In this way, the carbody structure becomes stiffer and the resonance frequency of the FBM can be increased beyond the upper limit of the discomfort range of frequency, improving the ride comfort. The theoretical principle of this method has been demonstrated employing a passenger rail vehicle model that includes the carbody as a free–free Euler–Bernoulli beam and the anti-bending bars as longitudinal springs jointed to the vertical supports. Also, the method feasibility has been verified in the past using an experimental scale demonstrator system. In this paper, a new model of the carbody–anti-bending bar system is proposed by including three-directional elastic elements (vertical and longitudinal direction and rotation in the vertical–longitudinal plane) to model the fastening of the anti-bending bars to the supports and the vertical motion of the anti-bending bars modelled as free–free Euler–Bernoulli beams connected to the elastic elements of the fastening. In the longitudinal direction, the anti-bending bars work as springs connected to the longitudinal elastic elements of the fastening. The modal analysis method is applied to point out the basic properties of the frequency response functions (FRFs) of the carbody–anti-bending bars system, considering the bounce and FBMs of both the carbody and the anti-bending bars. A parametric study of the FRF of the carbody shows that the vertical stiffness of the fastening should be sufficiently high enough to eliminate the influence of the modes of the anti-bending bars upon the carbody response and to reduce the anti-bending bars vibration in the frequency range of interest. Longitudinal stiffness of the elastic elements of the fastening is critical to increase the bending resonance frequency of the carbody out of the sensitive range. Longer anti-bending bars can improve the capability of the anti-bending bars to increase the bending resonance without the risk of interference effects caused by the bounce and bending modes of the anti-bending bars.

Keywords: carbody; anti-bending bars; Euler–Bernoulli beam; bounce mode; FBM; fastening stiffness

Academic Editor: Frédéric C. Lebon

Received: 4 December 2024
Revised: 7 January 2025
Accepted: 10 January 2025
Published: 12 January 2025

Citation: Apostol, I.-I.; Mazilu, T.; Dumitriu, M. Study on the Dynamic Response of the Carbody–Anti-Bending Bars System. *Technologies* **2025**, *13*, 31. https://doi.org/10.3390/technologies13010031

1. Introduction

Railway vehicles are subjected to a complex vibration behaviour coming from the 3D irregularity of the track [1–3], which affects the ride quality and comfort [4–6], the

traction-braking behaviour [7–9], and produces rolling surfaces wear and fatigue in the structure of the vehicle [10–12].

Much effort has been made to develop research to enhance the ride comfort regarding vertical vibration in passenger rail vehicles, especially in high-speed vehicles. High-speed vehicles must meet specific requirements that involve distinct approaches. For instance, high-speed vehicles should be lighter to reduce energy consumption and vibrations transmitted through the ground, resulting in lower manufacturing costs [13,14]. When this requirement is applied to a carbody with a long length, its structure becomes more flexible [15], causing intense structural vibration that affects the ride comfort and the life service because of material fatigue [16,17]. As for ride comfort, this deteriorates because the FBM of the light, long-length carbody, which is the most important regarding vibration behavior, has its eigenfrequency within the frequency range of maxim sensitivity of the human being [18–20].

Two main approaches have been developed to enhance the ride comfort in high-speed vehicles: (a) isolating the carbody by applying passive, semi-active, and active methods to diminish the transmittal of the vibration generated by track irregularity to the carbody via suspension [21–23]; and (b) reducing the structural vibration of the carbody by applying passive and active methods using specific devices mounted to the carbody [24–27].

Semi-active and active methods are based on the use of different types of actuators that require complex command and control systems and are therefore expensive and less reliable [28–30].

Passive methods involve the use of passive elements of suspension (springs and dashpots) or different mechanical devices that are simpler to make, less costly, and more reliable [31–33].

One of the passive methods of reducing the bending vibrations of light passenger rail carbody to enhance ride comfort involves the use of a carbody–anti-bending bars system [34]. This system has two bars mounted under the carbody chassis via vertical supports attached to the longitudinal beams of the chassis, and its aim is to increase the frequency of the FBM of the carbody over the upper limit of the sensitivity range of the human body to vertical vibrations.

Figure 1 shows how the carbody–anti-bending bars system works, where the carbody is labelled 1, the anti-bending bar is labelled 2, the supports are labelled 3, and the secondary suspension is labelled 4, which are displayed for simplicity. The carbody motion is induced by the motion of the bogies (not shown in the figure) z_{b1} and z_{b2} via the elements of the secondary suspension.

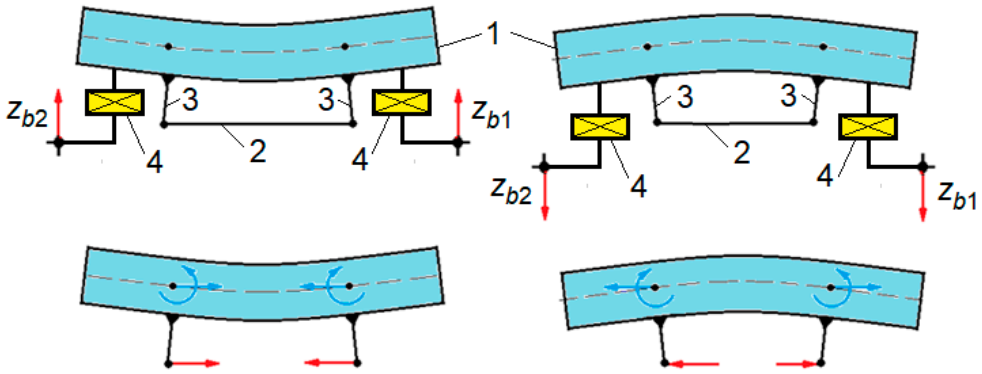

Figure 1. Principle of the carbody—anti-bending bars: 1. carbody; 2. anti-bending bar; 3. support; 4. secondary suspension; z_{b1} and z_{b2}—displacements imposed by the bogies.

When the FBM of the carbody is excited, the cross-sections in which the anti-bending bar supports are fixed, located on either side of the vertical axis of symmetry of the carbody,

rotate in opposite directions. Depending on how the carbody bends, the anti-bending bars are subjected to stretching or compression. In this way, longitudinal elastic reaction forces appear in the anti-bending bars acting on the supports (figured by red arrows), resulting in longitudinal forces and bending moments at the level of the neutral axis of the carbody. Bending moments are opposed to the bending motion of the carbody. These moments are of an elastic nature, and therefore their effect leads to an increase in the bending stiffness of the carbody and the eigenfrequency of its FBM.

To demonstrate the possibility of enhancing the ride comfort by increasing the eigenfrequency of the FBM of the carbody beyond the upper limit of the frequency range of maximum sensitivity to vertical vibrations with the aid of the anti-bending bar system, an original model of the railway vehicle with seven degrees of freedom was used in the cited reference. The carbody was represented as a free–free Euler–Bernoulli equivalent beam, and its rigid modes of vertical vibration and the FBM have been included in the vehicle model via the modal analysis method. The two bogies of the vehicle have been modelled as double-degree rigid objects, namely bounce and pitch. The anti-bending bars have been reduced to linear elastic elements articulated by supports, hereinafter referred to as the spring model. The mass of the anti-bending bars in relation to the weight of the carbody was neglected. The parameters of the anti-bending bars, respectively their length and diameter, are determined based on the condition to achieve a particular frequency of bending of the carbody with anti-bending bars, advantageous for comfort. However, to limit the interference between the bending vibration of the carbody and the bending vibration of the anti-bending bars, the maximum length of the bars has been set so that the FBM frequency of the anti-bending bars is one octave higher than the FBM of the carbody.

The feasibility of the method of improving the comfort of passenger vehicles by using the anti-bending bar system was proven via an experimental scale demonstrator system [35,36].

The objective of this paper is to deepen the research on the vertical vibrations of vehicles with anti-bending bars on the basis of the development of the model of the carbody–anti-bending bars system presented in [34]. A new model of the carbody–anti-bending bar system has been proposed by including the elastic elements for fastening the anti-bending bars of supports capable of relative vertical and longitudinal displacements and relative rotation in the vertical-longitudinal plane. The anti-bending bars are modelled as free–free Euler–Bernoulli beams that are connected at the ends by the elastic elements of the support fasteners. In this way, the model of the carbody–anti-bending bar system allows the description of the vertical bending movement of the anti-bending bars by considering the rigid modes and the FBM. On the longitudinal direction, the model of the anti-bending bars previously proposed in ref. [34] is preserved. The paper aims to highlight the basic properties of the carbody–anti-bending bar system regarding the following: (a) the correlation between the bounce and bending frequencies of the carbody–anti-bending bar system and the stiffness of the elastic elements of the fastening of the anti-bending bars to the supports; (b) the influence of the elastic elements of the fastening of the anti-bending bars by the supports on the FRFs; and (c) identifying opportunities to augment the frequency of carbody bending.

2. Mechanical Model of the Carbody–Anti-Bending Bar System and the Equations of Motion

Figure 2 shows the mechanical model of the carbody–anti-bending bars system, in which the vehicle carbody and the anti-bending bars are considered free–free Euler–Bernoulli beams. The anti-bending bars are attached to the vertical supports fixed to the carbody chassis longerons by elastic elements that work in three directions: verti-

cal translation, longitudinal translation along the anti-bending bars, and rotation in the vertical–longitudinal plane.

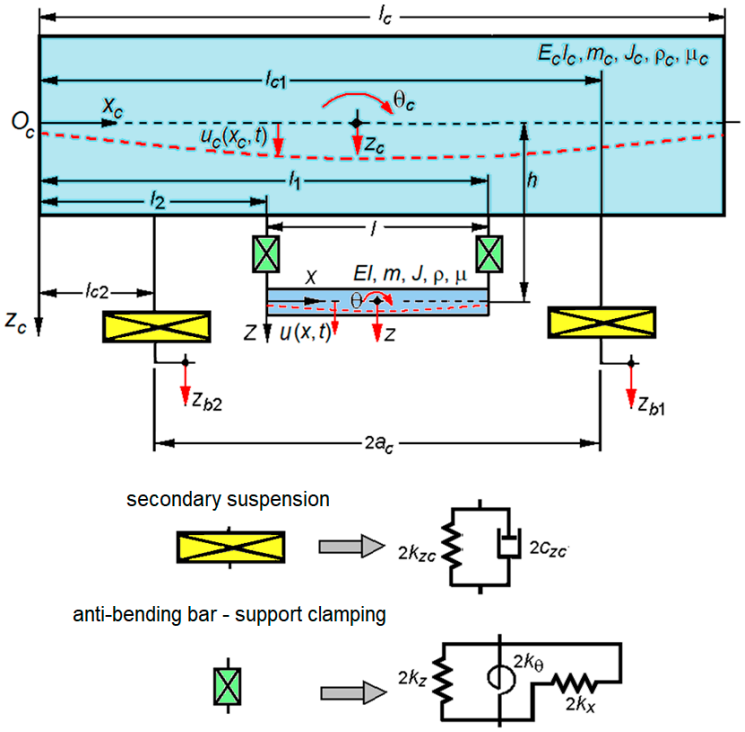

Figure 2. Mechanical model of the carbody—anti-bending bars system.

The carbody rests on the elements of the secondary suspension, which are modelled as Kelvin–Voigt systems working only in the vertical direction.

The parameters of the model are as follows: E_cI_c—the bending stiffness of the carbody, where E_c is the Young modulus and I_c is the second moment of area of the carbody cross-section; ρ_c—the carbody mass per unit length; μ_c—the structural damping coefficient of the carbody; l_c—the length of the carbody; $l_{c1,c2}$—the distances between the secondary suspension elements and the left end of the carbody; $2k_{zc}$—the elastic constant of the secondary suspension at one end of the carbody; $2c_{zc}$—the damping constant of the secondary suspension at one end of the carbody; EI—the bending stiffness of a bar, where E is the Young modulus and I is the second moment of area of the bar cross-section; ρ—the mass of one bar per unit length; μ—the structural damping coefficient of the bar; d—the diameter of a bar; l—the length of a bar; k_x—the longitudinal stiffness of the bar–support fastening; k_z—the vertical stiffness of the bar–support fastening; k_θ—the angular stiffness of the bar–support fastening for rotations in the vertical–longitudinal plane; $l_{1,2}$—the distances between the bar supports and the left end of the carbody; h—the distance between the anti–bending bars and the neutral axis of the carbody.

In the longitudinal direction, the anti-bending bars are reduced to elastic elements of stiffness k (for a bar) that work in series with the longitudinal elastic elements of the bars' attachment to their supports (Figure 3). The cumulative effect is an equivalent elastic element with the stiffness.

$$k_e = k\frac{k_x}{2k + k_x}. \quad (1)$$

The excitation of the carbody—anti-bending bars system comes from the vertical displacements of the bogies, $z_{b1,b2}$, which are applied at the level of the secondary suspension elements.

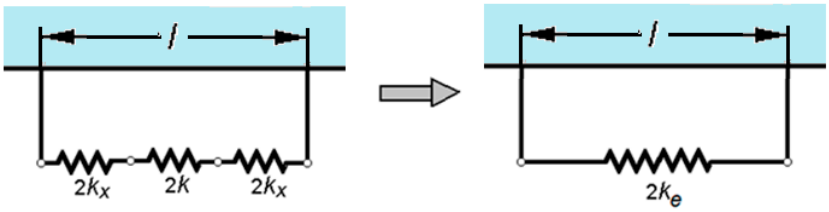

Figure 3. Mechanical model of the anti-bending bars in the longitudinal direction.

The motion of the carbody is described by the function $u_c(x_c, t)$, which represents the displacement of the x_c section at the time t with respect to the $O_c x_c z_c$ reference frame.

The motion of the anti-bending bars is described similarly by means of a single function of the form $u(x, t)$ since the two bars move identically due to the symmetry and the absence of the rolling motion of the carbody; x locates any section of the bar in relation to the Oxz reference system originating at the left end of the anti-bending bar, at the level of its neutral axis.

The presented model can be considered a simplified model of the railway vehicle, obtained by neglecting the components of the bogies and reducing them to simple vertical displacements imposed on the secondary suspension elements. However, the simplified vehicle model has the particularity of having the same fundamental properties as those of the complete vehicle model. The advantage of the simplified model lies in the possibility of easily establishing the correlation between the characteristics of the anti-bending bar—support clamping and evaluating the coupling between the anti-bending bar vibration and the carbody vibration.

Such an approach is not a new one. Cheli and Corradi used a similar model to analyse the excitation mechanism of the vibration modes of the carbody [37]. However, the simplified model of the vehicle adopted here is different from the one presented in the cited work above because of the anti-bending bar system. In addition, the problem addressed by Cheli and Corradi is totally different from the problem dealt with in this paper, as can be seen from the presentation above.

Figure 4 shows the loads acting on the carbody and Figure 5 displays the corresponding reactions acting on the anti-bending bars.

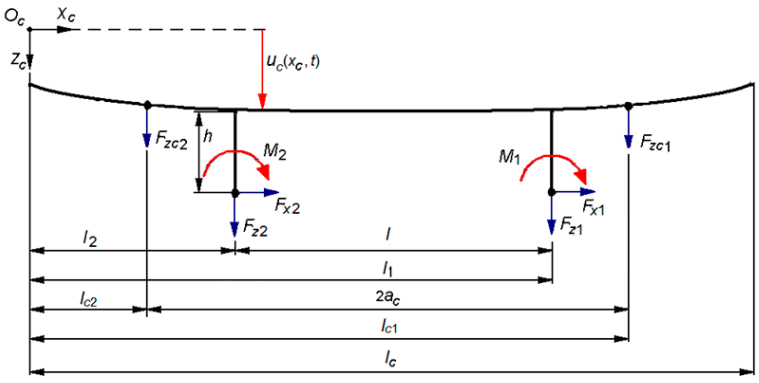

Figure 4. Loading the carbody.

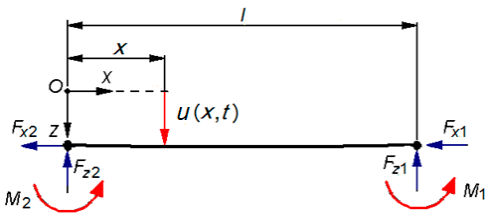

Figure 5. Loading the anti-bending bars.

Applying the free–free Euler–Bernoulli beam theory for both carbody and anti-bending bars, the equations of motion read as follows:

$$\begin{aligned} &E_c I_c \frac{\partial^4 u_c(x_c,t)}{\partial x_c^4} + \mu_c I_c \frac{\partial^5 u_c(x_c,t)}{\partial x_c^4 \partial t} + \rho_c \frac{\partial^2 u_c(x_c,t)}{\partial t^2} = \\ &\sum_{i=1}^{2} [F_{zci}\delta(x_c - l_{ci}) + F_{zi}\delta(x_c - l_i)] - \sum_{i=1}^{2} (M_i - F_{xi}h)\frac{\mathrm{d}\delta(x_c - l_i)}{\mathrm{d}x_c}, \end{aligned} \tag{2}$$

$$\begin{aligned} &2EI\tfrac{\partial^4 u(x,t)}{\partial x^4} + 2\mu I \tfrac{\partial^5 u(x,t)}{\partial x^4 \partial t} + 2\rho \tfrac{\partial^2 u(x,t)}{\partial t^2} = -F_{z1}\delta(x-l) - F_{z2}\delta(x) + \\ &M_1 \tfrac{\mathrm{d}\delta(x-l)}{\mathrm{d}x} + M_2 \tfrac{\mathrm{d}\delta(x)}{\mathrm{d}x}, \end{aligned} \tag{3}$$

where $\delta(.)$ is the Dirac delta function; F_{zci} are the forces in the secondary suspension; and F_{xi}, F_{zi}, and M_i are the forces and the moments in the elastic elements of the anti-bending bars—supports fastenings

$$F_{zci} = -2c_{zc}\left(\frac{\partial u_c(l_{ci},t)}{\partial t} - \dot{z}_{bi}\right) - 2k_{zc}[u_c(l_{ci},t) - z_{bi}], \tag{4}$$

$$\begin{aligned} &F_{x1,2} = \pm 2k_e h\left[\tfrac{\partial u_c(l_1,t)}{\partial x_c} - \tfrac{\partial u_c(l_2,t)}{\partial x_c}\right], \ . \\ &F_{z1} = -2k_z[u_c(l_1,t) - u(l,t)], \quad F_{z2} = -2k_z[u_c(l_2,t) - u(0,t)], \\ &M_1 = -2k_\theta\left[\tfrac{\partial u_c(l_1,t)}{\partial x_c} - \tfrac{\partial u(l,t)}{\partial x}\right], \quad M_2 = -2k_\theta\left[\tfrac{\partial u_c(l_2,t)}{\partial x_c} - \tfrac{\partial u(0,t)}{\partial x}\right] \ . \end{aligned} \tag{5}$$

Employing the modal analysis method, the displacement of the carbody and the displacement of the anti-bending bars can be described as follows.

$$u_c(x_c,t) = z_c(t) + \left(x_c - \frac{l_c}{2}\right)\theta_c(t) + Y_c(x_c)T_c(t), \tag{6}$$

where $z_c(t)$ and $\theta_c(t)$ are the bounce and pitch of the carbody, $T_c(t)$ and $Y_c(x_c)$ are the time coordinate and the eigenfunction of the FBM of the carbody, and we obtain the following:

$$u(x,t) = z(t) + \left(x - \frac{l}{2}\right)\theta(t) + Y(x)T(t), \tag{7}$$

where $z(t)$ and $\theta(t)$ are the bounce and pitch of the anti-bending bars, $T(t)$ and $Y(x)$ are the time coordinate and the eigenfunction of the FBM of the anti-bending bars.

The two eigenfunctions have similar shapes.

$$Y_c(x_c) = \sin(\alpha_c x_c) + \sinh(\alpha_c x_c) - \frac{\sin(\alpha_c l_c) - \sinh(\alpha_c l_c)}{\cos(\alpha_c l_c) - \cosh(\alpha_c l_c)}(\cos(\alpha_c x_c) - \cosh(\alpha_c x_c)), \tag{8}$$

$$Y(x) = \sin(\alpha x) + \sinh(\alpha x) - \frac{\sin(\alpha l) - \sinh(\alpha l)}{\cos(\alpha l) - \cosh(\alpha l)}(\cos(\alpha x) - \cosh(\alpha x)), \tag{9}$$

where $\alpha_c = \sqrt[4]{\frac{p_c^2 \rho_c}{E_c I_c}}$ and $\alpha = \sqrt[4]{\frac{p^2 \rho}{EI}}$ verify the following characteristic equations:

$$\cos \alpha_c l_c \cosh \alpha_c l_c - 1 = 0 \tag{10}$$

and

$$\cos \alpha l \cosh \alpha l - 1 = 0 \tag{11}$$

where p_c and p are the natural angular frequency of the FBM of the carbody and anti-bending bars.

Next, following the modal analysis method steps that are presented in the Appendix A, the following equations of motion can be distilled:

- For the bounce motion:

$$m_c\ddot{z}_c + 4c_{zc}\dot{z}_c + 4(k_{zc}+k_z)z_c + 4\varepsilon c_{zc}\dot{T}_c + 4(\varepsilon k_{zc}+\beta k_z)T_c - 4k_z z - 4\gamma k_z T = 2c_{zc}\left(\dot{z}_{b1}+\dot{z}_{b2}\right) + 2k_{zc}(z_{b1}+z_{b2}), \tag{12}$$

$$2m\ddot{z} + 4k_z z + 4\gamma k_z T - 4k_z z_c - 4\beta k_z T_c = 0, \tag{13}$$

- For the pitch motion:

$$J_c\ddot{\theta}_c + 4a_c^2 c_{zc} + (4a_c^2 k_{zc} + l^2 k_z + 4k_\theta)\theta_c - (l^2 k_z + 4k_\theta)\theta = 2a_c c_{zc}\left(\dot{z}_{b1}-\dot{z}_{b2}\right) + 2a_c k_{zc}(z_{b1}-z_{b2}), \tag{14}$$

$$2J\ddot{\theta} + (l^2 k_z + 4k_\theta)\theta - (l^2 k_z + 4k_\theta)\theta_c = 0, \tag{15}$$

- For the FBM:

$$m_{mc}\ddot{T}_c + (c_{mc}+4\varepsilon^2 c_{zc})\dot{T}_c + (k_{mc}+4\varepsilon^2 k_{zc}+4\beta^2 k_z+4\beta'^2 k_\theta+8\beta'^2 h^2 k_e)T_c + 4\varepsilon c_{zc}\dot{z}_c + (4\varepsilon k_{zc}+4\beta k_z)z_c - 4\beta k_z z - 4(\beta\gamma k_z - \beta'\gamma' k_\theta)T = 2\varepsilon c_{zc}(\dot{z}_{b1}+\dot{z}_{b2}) + 2\varepsilon k_{zc}(z_{b1}+z_{b2}), \tag{16}$$

$$2m_m\ddot{T} + 2c_m\dot{T} + 2(k_m + 2\gamma^2 k_z + 2\gamma'^2 k_\theta)T + 4\gamma k_z z - 4\gamma k_z z_c - 4(\beta\gamma k_z - \beta'\gamma' k_\theta)T_c = 0, \tag{17}$$

where m_{mc}, c_{mc}, and k_{mc} are the modal mass, damping, and stiffness for the FBM of the carbody and m_m, c_m, and k_m are the modal mass, damping, and stiffness associated to the first mode of the anti-bending bars.

$$m_{mc} = \rho_c\int_0^{l_c} Y_c^2 \mathrm{d}x_c,\ c_{mc} = \mu_c I_c\int_0^{l_c}\left(\frac{\mathrm{d}^2 Y_c}{\mathrm{d}x_c^2}\right)^2\mathrm{d}x_c,\ k_{mc} = E_c I_c\int_0^{l_c}\left(\frac{\mathrm{d}^2 Y_c}{\mathrm{d}x_c^2}\right)^2\mathrm{d}x_c, \tag{18}$$

$$m_m = \rho\int_0^{l} Y^2 \mathrm{d}x,\ c_m = \mu I\int_0^{l}\left(\frac{\mathrm{d}^2 Y}{\mathrm{d}x^2}\right)^2\mathrm{d}x,\ k_m = EI\int_0^{l}\left(\frac{\mathrm{d}^2 Y}{\mathrm{d}x^2}\right)^2\mathrm{d}x. \tag{19}$$

The following notations have been used in equations of motion (12)–(17):

$$\begin{aligned} &Y_c(l_{c1}) = Y_c(l_{c2}) = \varepsilon,\ Y_c(l_1) = Y_c(l_2) = \beta,\\ &\tfrac{\mathrm{d}Y_c(l_{c1})}{\mathrm{d}x_c} = -\tfrac{\mathrm{d}Y_c(l_{c2})}{\mathrm{d}x_c} = \varepsilon',\ \tfrac{\mathrm{d}Y_c(l_1)}{\mathrm{d}x_c} = -\tfrac{\mathrm{d}Y_c(l_2)}{\mathrm{d}x_c} = \beta',\\ &Y(0) = Y(l) = \gamma,\ \tfrac{\mathrm{d}Y(0)}{\mathrm{d}x} = -\tfrac{\mathrm{d}Y(l)}{\mathrm{d}x} = \gamma'. \end{aligned} \tag{20}$$

Examining equations of motion (12)–(17), there are two independent sets of equations of motion: (a) Equations (12) and (13) and (16) and (17) that describe symmetrical motions of bounce and bending; (b) Equations (14) and (15) for antisymmetric pitch motion.

Excitation of the carbody–anti-bending bar system has two modes of excitation: (a) symmetrical mode of excitation, implying the bogie displacements sum, $z_{b1} + z_{b2}$, which excites the symmetrical motions; (b) antisymmetric mode of excitation, involving the difference between the bogie displacements, $z_{b1} - z_{b2}$, exciting the antisymmetric motion.

3. Frequency Response Functions

To determine the FRFs, it is considered that both the excitation of the carbody–anti-bending bars system and its response are of the harmonic shape. It is presumed that the displacements z_{b1} and z_{b2} are harmonic functions of angular frequency ω with equal amplitudes. The two displacements are in phase to excite the symmetrical modes, written as follows:

$$z_{b1,2} = Z_b\cos\omega t \tag{21}$$

or out of phase to excite the antisymmetric modes, written as follows:

$$z_{b1,2} = \pm Z_b \cos \omega t \tag{22}$$

where Z_b is the amplitude.

The response of the carbody–anti-bending bars system is described by the following relations:

$$z_c = Z_c \cos(\omega t + \varphi_{z_c}), \theta_c = \Theta_c \cos(\omega t + \varphi_{\theta_c}),\ T_c = T_{co} \cos(\omega t + \varphi_{T_c}), \tag{23}$$

$$z = Z \cos(\omega t + \varphi_z),\ \theta = \Theta \cos(\omega t + \varphi_\theta),\ T = T_o \cos(\omega t + \varphi_T), \tag{24}$$

where Z_c, Θ_c, and T_{co}, and φ_{zc}, $\varphi_{\theta c}$, and φ_{Tc} are the amplitudes and the initial phases of the carbody coordinates, and Z, Θ, and T_o, and φ_z, φ_θ and φ_T are the amplitudes and the initial phases of the anti-bending bars coordinates.

Complex variables associated to the real ones are introduced with the following:

$$\overline{z}_{b1,2} = \overline{Z}_b e^{\omega t} \tag{25}$$

$$\overline{z}_c = \overline{Z}_c e^{i\omega t}, \overline{\theta}_c = \overline{\Theta}_c e^{i\omega t},\ \overline{T}_c = \overline{T}_{co} e^{i\omega t}, \tag{26}$$

$$\overline{z} = \overline{Z} e^{i\omega t}, \overline{\theta} = \overline{\Theta} e^{i\omega t},\ \overline{T} = \overline{T}_o e^{i\omega t}, \tag{27}$$

where the complex amplitudes are given by the relations, written as follows:

$$\overline{Z}_b = Z_b e^{i\times 0} \tag{28}$$

$$\overline{Z}_c = Z_c e^{i\varphi_{z_c}},\ \overline{\Theta}_c = \Theta_c e^{i\varphi_{\theta_c}},\ \overline{T}_{co} = T_{co} e^{i\varphi_{T_c}}, \tag{29}$$

$$\overline{Z} = Z e^{i\varphi_z},\ \overline{\Theta} = \Theta e^{i\varphi_\theta},\ \overline{T}_o = T_o e^{i\varphi_T}. \tag{30}$$

Complex variables verify the equations of motion, written as follows:

- Symmetrical modes:

$$\left[-\omega^2 m_c + 4i\omega c_{zc} + 4(k_{zc} + k_z)\right]\overline{Z}_c + 4(\varepsilon k_{zc} + \beta k_z + i\omega\varepsilon c_{zc})\overline{T}_c - 4k_z\overline{Z} - 4\gamma k_z\overline{T} = 4(i\omega c_{zc} + k_{zc})\overline{Z}_b \tag{31}$$

$$\left[-\omega^2 m_{mc} + i\omega(c_{mc} + 4\varepsilon^2 c_{zc}) + (k_{mc} + 4\varepsilon^2 k_{zc} + 4\beta^2 k_z + 4\beta'^2 k_\theta + 8\beta'^2 h^2 k_e)\right]\overline{T}_c + 4[i\omega\varepsilon c_{zc} + (\varepsilon k_{zc} + \beta k_z)]\overline{Z}_c - 4\beta k_z\overline{Z} - 4(\beta\gamma k_z - \beta'\gamma' k_\theta)\overline{T} = 4\varepsilon(i\omega c_{zc} + k_{zc})\overline{Z}_b \tag{32}$$

$$(-2\omega^2 m + 4k_z)\overline{Z} + 4\gamma k_z\overline{T} - 4k_z\overline{Z}_c - 4\beta k_z\overline{T}_c = 0 \tag{33}$$

$$\left[-2\omega^2 m_m + 2i\omega c_m + 2(k_m + 2\gamma^2 k_z + 2\gamma'^2 k_\theta)\right]\overline{T} - 4\gamma k_z\overline{Z}_c - 4(\beta\gamma k_z - \beta'\gamma' k_\theta)\overline{T}_c = 0. \tag{34}$$

- Antisymmetric modes:

$$\left[-\omega^2 J_c + 4i\omega a_c^2 c_{zc} + (4a_c^2 k_{zc} + l^2 k_z + 4k_\theta)\right]\overline{\Theta}_c - (l^2 k_z + 4k_\theta)\overline{\Theta} = 4(i\omega a_c c_{zc} + a_c k_{zc})\overline{Z}_b \tag{35}$$

$$\left[-2\omega^2 J\ddot{\theta} + (l^2 k_z + 4k_\theta)\right]\overline{\Theta} - (l^2 k_z + 4k_\theta)\overline{\Theta}_c = 0. \tag{36}$$

There are two sets of algebraic equations; the first has four equations, (31)–(34), and the second has 2 equations, (35) and (36), where the complex amplitudes are the unknowns. Solving the two sets of algebraic equations, the FRFs of the coordinates are obtained as follows:

- For symmetrical modes:

$$\overline{H}_{z_c}(\omega) = \frac{\overline{Z}_c(\omega)}{\overline{Z}_b},\ \overline{H}_{T_c}(\omega) = \frac{\overline{T}_c(\omega)}{\overline{Z}_b},\ \overline{H}_z(\omega) = \frac{\overline{Z}(\omega)}{\overline{Z}_b},\ \overline{H}_T(\omega) = \frac{\overline{T}(\omega)}{\overline{Z}_b}; \tag{37}$$

- For antisymmetric modes:

$$\overline{H}_{\theta_c}(\omega) = \frac{\overline{\Theta}_c(\omega)}{\overline{Z}_b},\ \overline{H}_\theta(\omega) = \frac{\overline{\Theta}(\omega)}{\overline{Z}_b}. \tag{38}$$

Finally, the FRFs of the displacement can be calculated as follows:

- For the carbody:

$$\overline{H}_c(x_c,\omega) = \overline{H}_{z_c}(\omega) + \left(x_c - \frac{l_c}{2}\right)\overline{H}_{\theta_c}(\omega) + Y_c(x)\overline{H}_{T_c}(\omega), \tag{39}$$

- For the anti-bending bars:

$$\overline{H}(x,\omega) = \overline{H}_z(\omega) + \left(x - \frac{l}{2}\right)\overline{H}_\theta(\omega) + Y(x)\overline{H}_T(\omega). \tag{40}$$

For comparison, the following two cases are considered: (a) carbody without anti-bending bars and (b) carbody with anti-bending bars—the spring model, as in ref. [34].

The FRFs of the coordinates for the carbody without anti-bending bars are obtained by solving Equations (31), (32), and (35) for $k_e = 0$, $k_z = 0$, and $k_\theta = 0$.

$$(-\omega^2 m_c + 4i\omega c_{zc} + 4k_{zc})\overline{Z}_c + 4(\varepsilon k_{zc} + i\omega\varepsilon c_{zc})\overline{T}_c = 4(i\omega c_{zc} + k_{zc})\overline{Z}_b \tag{41}$$

$$\left[-\omega^2 m_{mc} + i\omega(c_{mc} + 4\varepsilon^2 c_{zc}) + (k_{mc} + 4\varepsilon^2 k_{zc})\right]\overline{T}_c + 4(i\omega\varepsilon c_{zc} + \varepsilon k_{zc})\overline{Z}_c = 4\varepsilon(i\omega c_{zc} + k_{zc})\overline{Z}_b \tag{42}$$

$$(-\omega^2 J_c + 4i\omega a_c^2 c_{zc} + 4a_c^2 k_{zc})\overline{\Theta}_c = 4(i\omega a_c c_{zc} + a_c k_{zc})\overline{Z}_b \tag{43}$$

The FRFs of the coordinates for the carbody with anti-bending bars—the spring model—are obtained by solving Equations (31), (32), and (35) for $k_e = k$, $k_z = 0$, and $k_\theta = 0$.

$$(-\omega^2 m_c + 4i\omega c_{zc} + 4k_{zc})\overline{Z}_c + 4(i\omega\varepsilon c_{zc} + \varepsilon k_{zc})\overline{T}_c = 4(i\omega c_{zc} + k_{zc})\overline{Z}_b \tag{44}$$

$$\left[-\omega^2 m_{mc} + i\omega(c_{mc} + 4\varepsilon^2 c_{zc}) + (k_{mc} + 4\varepsilon^2 k_{zc} + 8\beta'^2 h^2 k)\right]\overline{T}_c + 4(i\omega\varepsilon c_{zc} + \varepsilon k_{zc})\overline{Z}_c = 4\varepsilon(i\omega c_{zc} + k_{zc})\overline{Z}_b \tag{45}$$

and Equation (43) for the pitch motion of the carbody.

4. Assessment of the Dynamic Response of the Carbody–Anti-Bending Bar System

In this section, the dynamic response of the carbody—anti-bending bar system is calculated and analysed based on the FRFs of the mechanical model presented above. Only the symmetrical modes are considered because the displacement at the centre of the carbody is the quantity of interest.

The reference values of the carbody model parameters are those mentioned in the reference [34], and these are presented in Table 1.

Table 1. Parameters of the carbody.

m_c = 34,000 kg	$2k_{zc}$ = 1.2 MN/m
$E_cI_c = 3.158 \times 10^9$ Nm^2	$2c_{zc}$ = 34.28 kNs/m
l_c = 26.4 m	m_{mc} = 35,224 kg
$2a_c$ = 19 m	k_{mc} = 88.998 MN/m
l_{c1} = 22.7 m	c_{mc} = 53.117 kNs/m
l_{c2} = 3.7 m	h = 1.2 m;

Anti-bending bars parameters are given in Table 2. The main parameters, l = 5.28 m and d = 0.17 m, are taken from ref. [34].

Table 2. Parameters of the anti-bending bars.

m = 941 kg	m_m = 975 kg
E = 210 GPa	k_m = 30.33 MN/m
l = 5.28 m	c_m = 860 Ns/m
d = 0.17 m	l_1 = 15.84 m
$I = 4.0998 \times 10^{-5}$ m^4	l_2 = 10.56 m
k = 902.76 MN/m	

Figure 6 shows the FRF of the displacement of the middle of the carbody without and with anti-bending bars—the spring model, calculated in the absence of damping. It is about

the two reference cases. The dynamic characteristic of the carbody is henpecked by the two peaks that correspond to the resonance frequencies of the carbody on the secondary suspension, whose movement presents only two degrees of freedom in the middle of the carbody due to the pitch motion not being present. Resonance frequencies of the carbody without anti-bending bars are given by the bounce mode at 1.328 Hz and by the FBM at 8.058 Hz. When the carbody is equipped with anti-bending bars, the resonance frequency of the FBM reaches up to 14.05 Hz, while the resonance frequency of the bounce mode remains unchanged at 1.334 Hz.

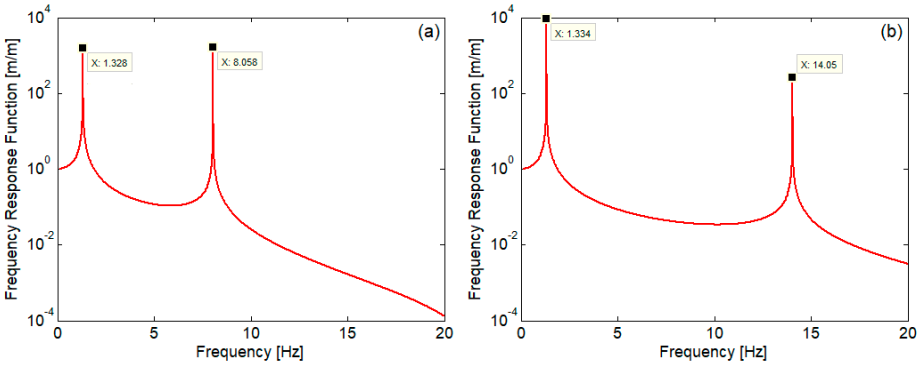

Figure 6. FRF in the centre of the carbody (reference cases): (**a**) carbody without anti-bending bars; (**b**) carbody with anti-bending bars (spring model).

In the following lines, the anti-bending bar modes and the stiffness of the fastening of the anti-bending bars to supports are considered. First, the longitudinal elasticity of the fastening of the anti-bending bars to supports is neglected, meaning $k_x \to \infty$ or $k_e = k$.

For simplicity, the angular stiffness k_θ is calculated depending on the vertical stiffness k_z, written as follows:

$$k_\theta = k_z \frac{b^2}{12}, \tag{46}$$

where b is the fastening width. Fastening width depends on the anti-bending bar diameter, and, as a guideline, it is considered $b = 1.3 \times d$.

Figure 7 shows the dynamic response in the centre of the carbody and in the middle of the anti-bending bars for several values of the vertical stiffness of the fastening of the anti-bending bars to the supports. Damping is not considered yet. The calculation was performed on the frequency range 0.1–100 Hz by discretising it with the step $\Delta f = 10$ μHz. All diagrams show 4 peaks corresponding to the four resonance frequencies of the system. However, the FRF in the centre of the carbody does not apparently show the fourth peak in diagrams (a) and (b). This is because the discretisation step is too large to catch the resonance peak due to the very poor coupling between the carbody vibration and that of the anti-bending bars, caused by the high elasticity of the fastening system. Indeed, by choosing a low enough frequency step, one can highlight the fourth resonance frequency, as Figure 8 shows. Here, the frequency step is 0.1 μHz, and the fourth resonance frequency appears in the FRF of the displacement at the centre of the carbody between 28.115 and 28.1155 Hz for $k_z = 10$ kN/m and between 28.460 and 28.465 Hz for $k_z = 100$ kN/m.

When the coupling between the carbody vibration and the anti-bending bars vibration is stronger, as seen in Figure 7c,d, practically only the resonance frequencies of the anti-bending bars are changed while the resonance frequencies of the carbody remain almost unchanged. Thus, the resonance frequency of the anti-bending bars bounce reaches 6.597 Hz for $k_z = 1$ MN/m and 11.08 Hz for $k_z = 10$ MN/m. At the same time, the resonance frequency of the bending of the anti-bending bars increases first to 31.91 Hz ($k_z = 1$ MN/m) and then to 58.40 Hz ($k_z = 10$ MN/m).

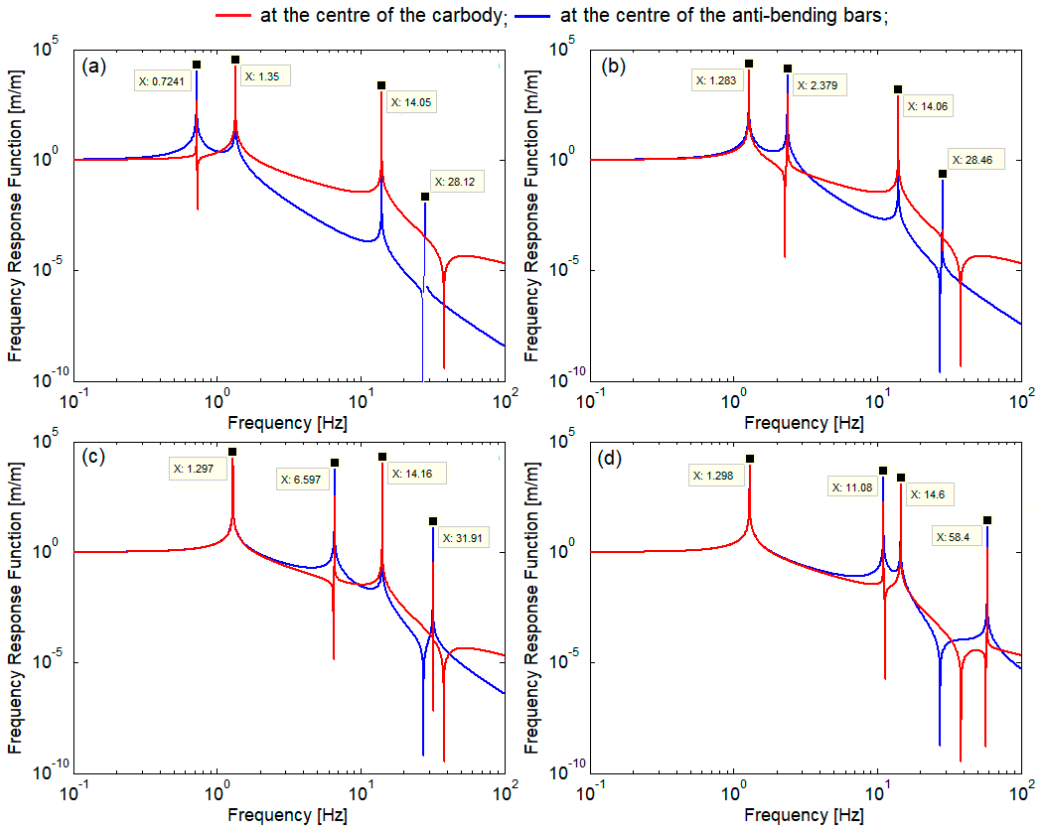

Figure 7. FRF (without damping): (**a**) k_z = 10 kN/m; (**b**) k_z = 100 kN/m; (**c**) k_z = 1 MN/m; (**d**) k_z = 10 MN/m.

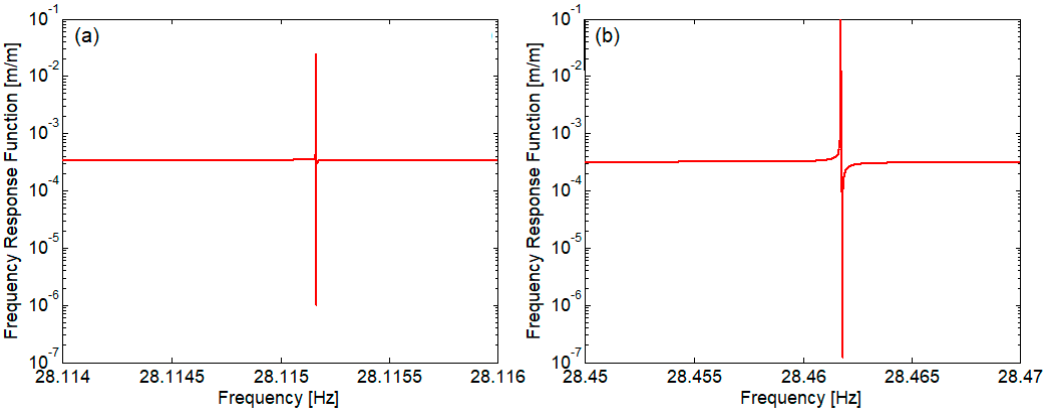

Figure 8. Detail of the FRF at the centre of the carbody (model without damping): (**a**) k_z = 10 kN/m; (**b**) k_z = 100 kN/m.

Figure 9 shows the FRFs in the middle of the carbody and in the centre of the anti-bending bars when the stiffness of the fastening of the anti-bending bars to the supports takes high values. The diagrams show the response functions also in the range of 0.1 to 100 Hz, without considering the influence of damping. In diagrams (a), (b), and (c) of Figure 9, the FRFs show three peaks corresponding to the resonance frequencies due to the bounce and bending of the carbody and the bounce of the anti-bending bars. The fourth peak, which is due to the bending of the anti-bending bars, is located outside the range considered for simulation. Diagram (d) shows only the resonance peaks of the carbody, the bounce of the anti-bend bars being outside the frequency range represented.

Based on the analysis of the frequency response of the carbody and the anti-bending bars calculated with the non-damping model, it is concluded that the resonance frequencies of the carbody on the secondary suspension are not significantly influenced by the presence of the anti-bending bars or by the vertical and rotational stiffness of the fastening of the anti-bending bars to the supports. On the flip side, the resonance frequencies of anti-bending bars increase continuously as the fastening of the anti-bending bars to the supports is stiffer. The justification comes from the fact that the mass of the carbody is much greater than the mass of the anti-bending bars, and its movement is slightly influenced by the presence of the anti-bending bars. On the other hand, the restriction imposed on the length of the anti-bending bars, resulting from the requirement that the resonance frequency at bending the anti-bending bars is no less than one octave from the resonance frequency at bending the carbody, is not necessary when the stiffness of the fastening of the anti-bending bars to the supports is sufficiently high, because their bending frequency increases with the stiffness of the fastening of the anti-bending bars to the supports.

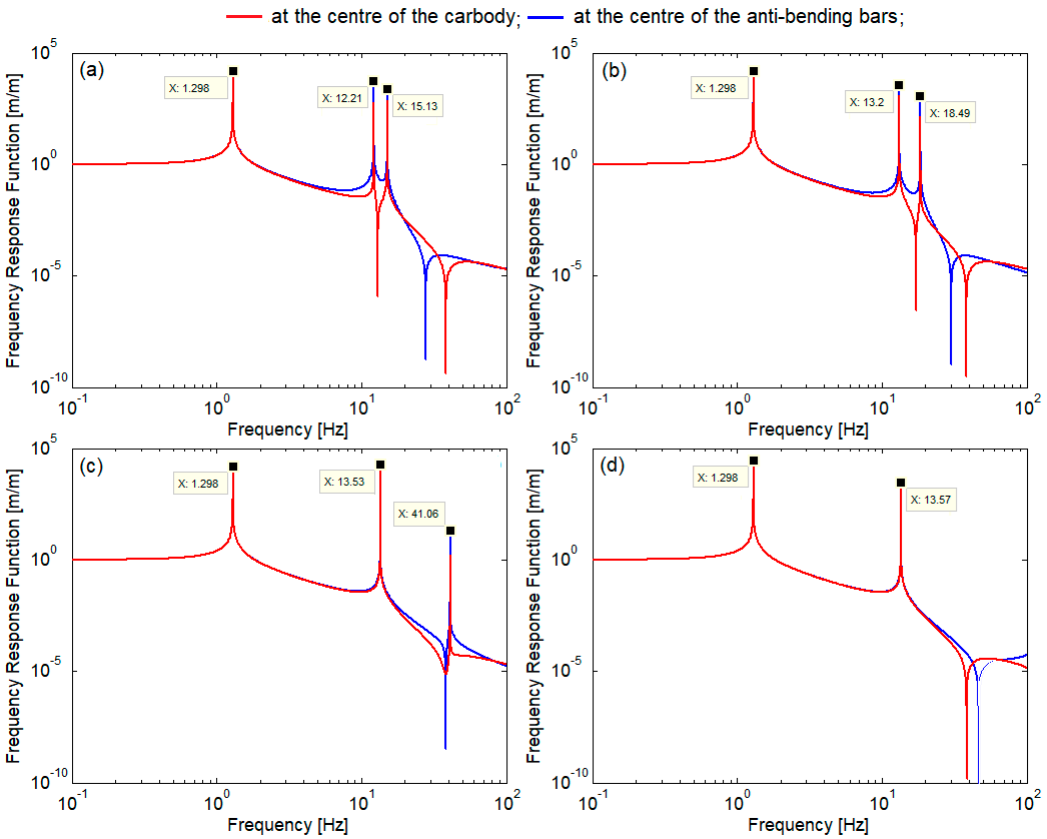

Figure 9. FRF (without damping): (**a**) k_z = 100 MN/m; (**b**) k_z = 1 GN/m; (**c**) k_z = 10 GN/m; (**d**) k_z = 100 GN/m.

Figures 10 and 11 show the influence of the model's damping on the FRFs of the carbody and anti-bending bars. It is about the damping of the secondary suspension, as well as the structural damping of the carbody and the anti-bending bars. For comparison, the FRF of the carbody without/with anti-bending bars is presented; in the latter case, the non-inertia bar type model was used. The effect of the anti-bending bars (spring model) on the frequency response is observed by increasing the bending frequency of the carbody from 8 Hz to 14 Hz.

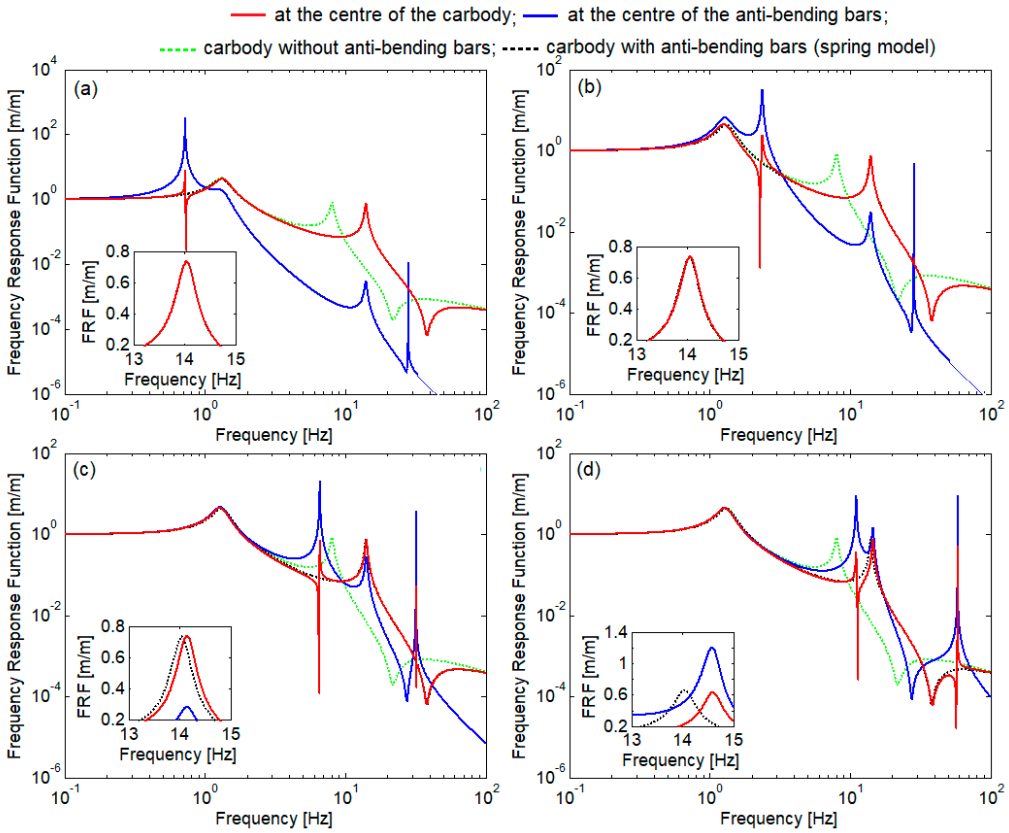

Figure 10. FRF (with damping): (**a**) k_z = 10 kN/m; (**b**) k_z = 100 kN/m; (**c**) k_z = 1 MN/m; (**d**) k_z = 10 MN/m.

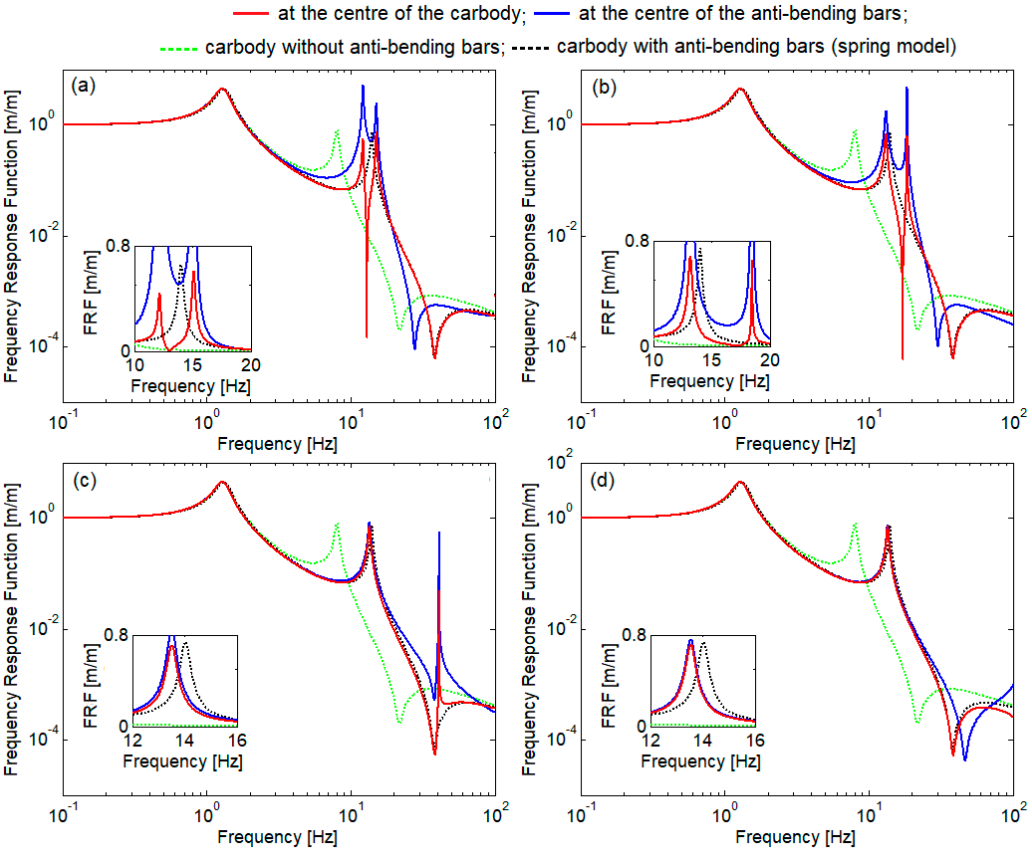

Figure 11. FRF (with damping): (**a**) k_z = 100 MN/m; (**b**) k_z = 1 GN/m; (**c**) k_z = 10 GN/m; (**d**) k_z = 100 GN/m.

In the case of low stiffness of the fastening between the anti-bending bars and the supports, Figure 10a,b, the frequency response curve in the middle of the carbody overlaps that calculated utilising the anti-bending bars (spring model), except for the area around the bounce frequency of the anti-bending bars. The vibration behaviour of the anti-bending bars is much more intense than that of the carbody in the low-frequency range due to the bounce resonance of the bars. At the same time, the vibration of the anti-bending bars has a poor damping at the bending frequency of approx. 28 Hz.

When the vibrations of the carbody and anti-bending bars are more stronger coupled (Figure 10c,d), the characteristics of the FRFs of the carbody–anti-bending bars system mentioned above are preserved, with the difference that the vibration of the anti-bending bars decreases in intensity at its bounce frequency but increases in the rest, especially at its bending resonance. In diagram (c), the vibration of the anti-bending bars is lower than that of the carbody at the bending frequency of the carbody, while in diagram (d), when the bounce of the anti-bending bars comes closer to the bending frequency of the carbody, the vibration of the anti-bending bars is greater than that of the carbody. It is also interesting to note that the bending resonance of the carbody increases to a certain extent compared to the ideal case where the carbody model is "fitted" with spring-type anti-bending bars. This aspect is the effect of the coupling between the bounce mode of the anti-bending bars and the bending mode of the carbody and it is especially visible in diagram (d), where the vertical stiffness of the fastening of the anti-bending bars to the supports is 10 MN/m.

When the vertical stiffness of the fastening of the anti-bending bars to the supports is higher, for instance, k_z = 100 MN/m and k_z = 1 GN/m, the bounce resonance of the anti-bending bars is near the bending resonance of the carbody, according to Figure 11a,b. The vibration of the carbody has two peaks between 10 Hz and 20 Hz, and both peaks are lower than the peak calculated with the help of the spring model of the anti-bending bars (dotted black line). The vibration of the anti-bending bars is more intense than that of the carbody when the excitation frequency is around the two peaks.

Diagrams (c) and (d) from Figure 11 present the FRFs for the case of very rigid fastening of the anti-bending bars to the supports. In diagram (c), where k_z = 10 GN/m, the FRFs of the carbody—anti-bending bars system have three peaks, of which the one located at the highest frequency corresponds to the bounce of the anti-bending bars, and in diagram (d), where k_z = 100 GN/m, these functions have only two peaks because the bounce of the anti-bending bars is out of the range of interest. As regards the vibration of the carbody, the results obtained are close to those obtained with the spring model of the anti-bending bars with two differences: (a) the peak related to the bending of the carbody has a slightly lower frequency, 13.51 Hz compared to 14.05 Hz resulting from the spring model of the anti-bending bars; (b) the vibration of the carbody shows the apex corresponding to the bounce of the anti-bending bars, as shown in diagram (c). The vibration of the anti-bending bars is practically equal to that of the carbody at low frequencies, up to 4–5 Hz, after which, progressively, it becomes higher.

Next, the influence of the longitudinal stiffness of the fastening of the anti-bending bars to the supports is analysed. The longitudinal stiffness of the fastening is linked to the longitudinal stiffness of the anti-bending bar k by a relationship of the shape.

$$k_x = Kk, \tag{47}$$

where K is a proportionality factor.

Figure 12 shows the FRFs in the centre of the carbody for different values of the stiffness fastening of the anti-bending bars to the supports, from 0 up to 30 Hz. The parametric calculation was carried out by choosing the last four values of the vertical stiffness of the fastening between the anti-bending bars and the supports considered in the previous case, so that the bounce frequency of the anti-bending bars is higher than the bending

frequency of the carbody. For each value of the vertical stiffness of the fastening of the anti-bending bars to the supports, five values of the longitudinal stiffness k_x corresponding to the proportionality factor K are tested.

$$K \in \{0.5,\ 1,\ 2,\ 5,\ \infty\} \tag{48}$$

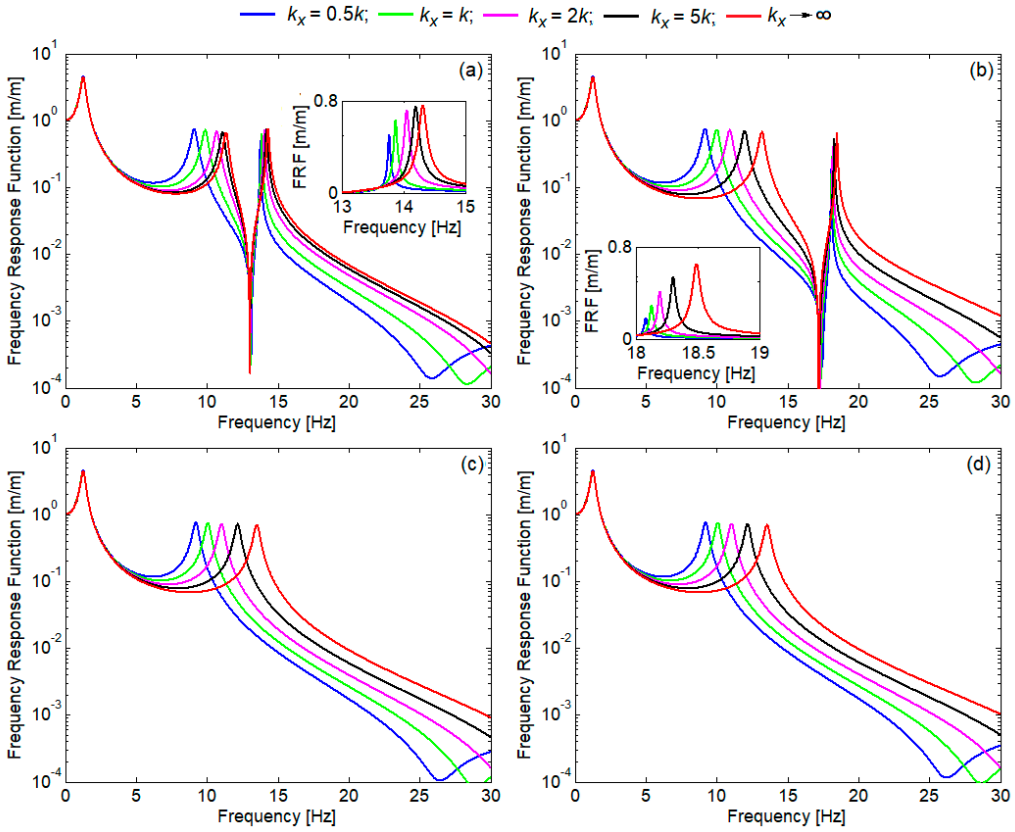

Figure 12. FRFs of displacement to the centre of the carbody for different values of the stiffness of the fastening of the anti-bending bars to the supports: (**a**) k_z = 100 MN/m; (**b**) k_z = 1 GN/m; (**c**) k_z = 10 GN/m; (**d**) k_z = 100 GN/m.

In diagrams (a) and (b) in Figure 12, both the peaks representing the bending resonance of the carbody and the bounce resonance of the anti-bending bars are close to each other. In diagrams (c) and (d), the peak of the bounce resonance of the anti-bending bars exceeds the limit of the frequency range presented. When the longitudinal stiffness of the fastening of the anti-bending bars to the support decreases, the peak frequency of the bounce resonance of the anti-bending bars decrease as the details in the diagrams (a) and (b) show. On the other hand, in all cases shown in Figure 12, the frequency of the peak corresponding to the bending resonance of the carbody decreases too as the longitudinal stiffness of the fastening becomes lower. The frequency values of these peaks are listed in Table 3.

Table 3. Carbody bending resonance frequency.

Vertical Stiffness k_z	**Proportionality Factor K**				
	∞	**5**	**2**	**1**	**0.5**
100 MN/m	12.20 Hz	11.51 Hz	10.07 Hz	9.88 Hz	9.11 Hz
1 GN/m	13.21 Hz	11.98 Hz	10.93 Hz	10.00 Hz	9.18 Hz
10 GN/m	13.52 Hz	12.16 Hz	11.04 Hz	10.07 Hz	9.22 Hz
100 GN/m	13.56 Hz	12.19 Hz	11.05 Hz	10.08 Hz	9.23 Hz

If the vertical stiffness k_z is 100 MN/m, then the bending frequency of the carbody decreases from 12.2 Hz to 9.11 Hz, and for k_z = 1 GN/m, the same frequency decreases from

13.2 Hz to 9.18 Hz. Regarding the last two cases considered, no important differences can be identified between them; the bending frequency of the carbody decreases from approx. 13.5 Hz to about 9.2 Hz.

On the other hand, when the longitudinal stiffness of the fastening equals $k_x = 0.2\,k$, which means $K = 0.5$, the frequency of the bending resonance of the carbody is between 9.11 and 9.23 Hz, whatever the vertical stiffness of the fastening.

In any case, the results obtained show the importance of ensuring longitudinal stiffness at a sufficiently high level so as not to compromise the functionality of the anti-bending bar system.

The effect of increasing the length of anti-bending bars on the FRFs of the carbody is further analysed. The analysis is restricted to one value of the vertical stiffness of the fastening, $k_z = 10$ GN/m, and two cases regarding the proportional factor K, respectively $K = 2$ and $K = 5$.

Figure 13 shows the FRF of the carbody for five values of the length of the anti-bending bars in arithmetic progression with a ratio of 0.8 m starting from a reference value of 5.28 m. Diagram (a) is constructed for $K = 2$, and the diagram (b), for $K = 5$, and the blue curve represents the reference FRF of the carbody. As the length of the anti-bending bars is longer, the bounce mode frequency of the bars decreases because the mass of the anti-bending bars increases. On the other hand, the effect of increasing the length of the anti-bending bars on the bending frequency of the carbody can be observed in both cases represented. For $K = 2$, the frequency of the carbody bending increases from 11.04 Hz to 11.84, and when $K = 5$, this frequency grows from 12.16 Hz for $l = 5.28$ m to 13.14 Hz for $l = 8.48$ m.

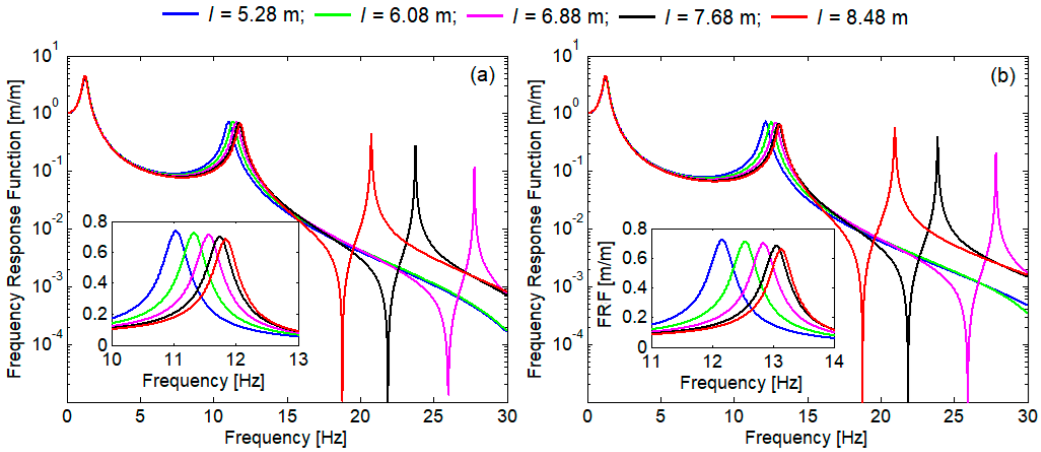

Figure 13. Influence of the length of anti-bending bars on FRF of the carbody: (**a**) $K = 2$; (**b**) $K = 5$.

5. Conclusions

In this work, a simplified model of the vehicle comprising the carbody resting on the secondary suspension and fitted with a system of anti-bending bars has been elaborated to explore the basic properties of the FRFs of the carbody–anti-bending bars system and to investigate the effectiveness of the bending vibration of the anti-bending bars and the stiffness of the fastening of the anti-bending bars to the supports upon the FRF of the carbody. To this aim, both carbody and anti-bending bars have been modelled as free–free Euler–Bernoulli beams, considering the rigid and FBMs and the vertical, longitudinal, and rotational stiffness in the vertical–longitudinal plane of the fastening of the anti-bending bars to the supports. The parametric study performed in this paper resulted in the following successive outcomes:

(a) In general, the vibration of the carbody is influenced by the interference with the bounce mode of the anti-bending bars, but it becomes independent when the vertical stiffness of the fastening is high enough;

(b) The vibration of the anti-bending bars is significantly higher than the carbody vibration because of their bounce and bending resonances when the vertical stiffness of the fastening is not sufficiently strong enough;
(c) To cut down the vibration of the anti-bending bars, high vertical stiffness in the fastening of the anti-bending bars to the supports is necessary;
(d) The resonance frequencies of the bounce and bending modes of the anti-bending bars continuously increase as the vertical stiffness of the fastening of the anti-bending bars to the supports is stiffer;
(e) The longitudinal elasticity of the fastening of the anti-bending bars to the supports reduces the bending frequency of the carbody and can even compromise the capability of the anti-bending bar system to raise the bending frequency of the carbody out of the sensitivity range;
(f) Compensation for the unfavorable influence of the longitudinal elasticity of the fastening of the anti-bending bars to the supports can be made by adopting longer anti-bending bars.

Further research aims to integrate the new model of the carbody–anti-bending bars system into the model of the entire passenger vehicle running on a track with random irregularity to assess the influence of this system upon the ride quality and ride comfort and to identify the possibilities to improve the vehicle performance.

Author Contributions: Conceptualization, T.M. and I.-I.A.; methodology, T.M. and M.D.; software, T.M. and I.-I.A.; validation, T.M., M.D. and I.-I.A.; formal analysis, T.M. and M.D.; investigation, I.-I.A., T.M. and M.D.; resources, M.D. and I.-I.A.; data curation, I.-I.A.; writing—original draft preparation, T.M. and I.-I.A.; writing—review and editing, M.D.; visualization, I.-I.A.; supervision, T.M.; project administration, T.M. All authors have read and agreed to the published version of the manuscript.

Funding: This research was funded by a grant from the National Program for Research of the National Association of Technical Universities—GNAC ARUT 2023, contract no. 154/04.12.2023.

Institutional Review Board Statement: Not applicable.

Informed Consent Statement: Not applicable.

Data Availability Statement: Data are contained within the article.

Acknowledgments: Not applicable.

Conflicts of Interest: The authors declare no conflicts of interest.

Appendix A

Displacements of the carbody and anti-bending bars, Equations (6) and (7), are introduced in the following equations of motion (Equations (2) and (3)):

$$E_c I_c \frac{\mathrm{d}^4 Y_c}{\mathrm{d}x_c^4} T_c + \mu_c I_c \frac{\mathrm{d}^4 Y_c}{\mathrm{d}x_c^4} \dot{T}_c + \rho_c \left[\ddot{z}_c + \left(x_c - \frac{l_c}{2} \right) \ddot{\theta}_c + Y_c \ddot{T}_c \right] = \sum_{i=1}^{2} \left[F_{zci} \delta(x_c - l_{ci}) + F_{zi} \delta(x_c - l_i) \right] - \sum_{i=1}^{2} (M_i - h F_{xi}) \frac{\mathrm{d}\delta(x_c - l_i)}{\mathrm{d}x_c}, \tag{A1}$$

$$2EI \frac{\mathrm{d}^4 Y}{\mathrm{d}x^4} T + 2\mu I \frac{\mathrm{d}^4 Y}{\mathrm{d}x^4} \dot{T} + 2\rho \left[\ddot{z} + \left(x - \tfrac{l}{2} \right) \ddot{\theta} + Y \ddot{T} \right] = -F_{z1} \delta(x - l) - F_{z2} \delta(x) + M_1 \frac{\mathrm{d}\delta(x-l)}{\mathrm{d}x} + M_2 \frac{\mathrm{d}\delta(x)}{\mathrm{d}x}. \tag{A2}$$

Equation (A1) is integrated on the interval $[0, l_c]$ and Equation (A2) is integrated on the interval $[0, l]$.

$$E_cI_cT_c\int_0^{l_c}\frac{\mathrm{d}^4Y_c}{\mathrm{d}x_c^4}\mathrm{d}x_c+\mu_cI_c\dot{T}_c\int_0^{l_c}\frac{\mathrm{d}^4Y_c}{\mathrm{d}x_c^4}\mathrm{d}x_c+\rho_c\ddot{z}_c\int_0^{l_c}\mathrm{d}x_c+\rho_c\ddot{\theta}_c\int_0^{l_c}\left(x_c-\frac{l_c}{2}\right)\mathrm{d}x_c+\rho_c\ddot{T}_c\int_0^{l_c}Y_c\mathrm{d}x_c=$$
$$=\sum_{i=1}^{2}\left[F_{zci}\int_0^{l_c}\delta(x_c-l_{ci})\mathrm{d}x_c+F_{zi}\int_0^{l_c}\delta(x_c-l_i)\mathrm{d}x_c\right]-\sum_{i=1}^{2}\left[(M_i-hF_{xi})\int_0^{l_c}\frac{\mathrm{d}\delta(x_c-l_i)}{\mathrm{d}x_c}\mathrm{d}x_c\right] \tag{A3}$$

$$2\left[EIT\int_0^{l}\frac{\mathrm{d}^4Y}{\mathrm{d}x^4}\mathrm{d}x+\mu I\dot{T}\int_0^{l}\frac{\mathrm{d}^4Y}{\mathrm{d}x^4}\mathrm{d}x+\rho\ddot{z}\int_0^{l}\mathrm{d}x+\rho\ddot{\theta}\int_0^{l}\left(x-\frac{l}{2}\right)\mathrm{d}x+\rho\ddot{T}\int_0^{l}Y\mathrm{d}x\right]=$$
$$-F_{z1}\int_0^{l}\delta(x-l)\mathrm{d}x-F_{z2}\int_0^{l}\delta(x)\mathrm{d}x+M_1\int_0^{l}\frac{\mathrm{d}\delta(x-l)}{\mathrm{d}x}\mathrm{d}x-M_2\int_0^{l}\frac{\mathrm{d}\delta(x)}{\mathrm{d}x}\mathrm{d}x. \tag{A4}$$

Performing the integrals, the following equations of motion for the carbody and anti-bending bars bounce are obtained:

$$m_c\ddot{z}_c=\sum_{i=1}^{2}(F_{zci}+F_{zi}), \tag{A5}$$

$$2m\ddot{z}=-(F_{z1}+F_{z2}), \tag{A6}$$

where the following results established by direct integration were considered:

$$\int_0^{l_c}\frac{\mathrm{d}^4Y_c}{\mathrm{d}x_c^4}\mathrm{d}x_c=0,\ \int_0^{l_c}\mathrm{d}x_c=l_c,\ \int_0^{l_c}\left(x_c-\frac{l_c}{2}\right)\mathrm{d}x_c=0,\ \int_0^{l_c}Y_c\mathrm{d}x_c=0,\ \int_0^{l_c}\delta(x_c-l_{ci})\mathrm{d}x_c=1,$$
$$\int_0^{l_c}\delta(x_c-l_i)\mathrm{d}x_c=1,\ \int_0^{l_c}\frac{\mathrm{d}\delta(x-l_{ci})}{\mathrm{d}x_c}\mathrm{d}x_c=0,\ \int_0^{l_c}\frac{\mathrm{d}\delta(x_c-l_i)}{\mathrm{d}x_c}\mathrm{d}x_c=0, \tag{A7}$$

and

$$\int_0^{l}\frac{\mathrm{d}^4Y}{\mathrm{d}x^4}\mathrm{d}x=0,\ \int_0^{l}\mathrm{d}x=l,\ \int_0^{l}\left(x-\frac{l}{2}\right)\mathrm{d}x=0,\ \int_0^{l}Y\mathrm{d}x=0,\ \int_0^{l}\delta(x-l)\mathrm{d}x=1,$$
$$\int_0^{l}\delta(x)\mathrm{d}x=1,\ \int_0^{l}\frac{\mathrm{d}\delta(x-l)}{\mathrm{d}x}\mathrm{d}x=0,\ \int_0^{l}\frac{\mathrm{d}\delta(x)}{\mathrm{d}x}\mathrm{d}x=0. \tag{A8}$$

To obtain the pitch equations, multiply Equation (A1) by $(x_c-l_c/2)$, and Equation (A2) by $(x-l/2)$, and then integrate each equation on the related domain, written as follows:

$$E_cI_cT_c\int_0^{l_c}\left(x_c-\frac{l_c}{2}\right)\frac{\mathrm{d}^4Y_c}{\mathrm{d}x_c^4}\mathrm{d}x_c+\mu_cI_c\dot{T}_c\int_0^{l_c}\left(x_c-\frac{l_c}{2}\right)\frac{\mathrm{d}^4Y_c}{\mathrm{d}x_c^4}\mathrm{d}x_c+\rho_c\ddot{z}_c\int_0^{l_c}\left(x_c-\frac{l_c}{2}\right)\mathrm{d}x_c+$$
$$\rho_c\ddot{\theta}_c\int_0^{l_c}\left(x_c-\frac{l_c}{2}\right)^2\mathrm{d}x_c+\rho_c\ddot{T}_c\int_0^{l_c}\left(x_c-\frac{l_c}{2}\right)Y_c\mathrm{d}x_c=$$
$$\sum_{i=1}^{2}\left[F_{zci}\int_0^{l_c}\left(x_c-\frac{l_c}{2}\right)\delta(x_c-l_{ci})\mathrm{d}x_c+F_{zi}\int_0^{l_c}\left(x_c-\frac{l_c}{2}\right)\delta(x_c-l_i)\mathrm{d}x_c\right]$$
$$-\sum_{i=1}^{2}\left[(M_i-hF_{xi})\int_0^{l_c}\left(x_c-\frac{l_c}{2}\right)\frac{\mathrm{d}\delta(x_c-l_i)}{\mathrm{d}x_c}\mathrm{d}x_c\right], \tag{A9}$$

$$2\left[EIT\int_0^{l}\left(x-\frac{l}{2}\right)\frac{\mathrm{d}^4Y}{\mathrm{d}x^4}\mathrm{d}x+\mu I\dot{T}\int_0^{l}\left(x-\frac{l}{2}\right)\frac{\mathrm{d}^4Y}{\mathrm{d}x^4}\mathrm{d}x+\rho\ddot{z}\int_0^{l}\left(x-\frac{l}{2}\right)\mathrm{d}x\right]+$$
$$2\left[\rho\ddot{\theta}\int_0^{l}\left(x-\frac{l}{2}\right)^2\mathrm{d}x+2\rho\ddot{T}\int_0^{l}\left(x-\frac{l}{2}\right)Y\mathrm{d}x\right]=-F_{zc1}\int_0^{l}\left(x-\frac{l}{2}\right)\delta(x-l)\mathrm{d}x-$$
$$-F_{zc2}\int_0^{l}\left(x-\frac{l}{2}\right)\delta(x)\mathrm{d}x+M_1\int_0^{l}\left(x-\frac{l}{2}\right)\frac{\mathrm{d}\delta(x-l)}{\mathrm{d}x}\mathrm{d}x+M_2\int_0^{l}\left(x-\frac{l}{2}\right)\frac{\mathrm{d}\delta(x)}{\mathrm{d}x}\mathrm{d}x. \tag{A10}$$

The integrals of the two equations are calculated either by direct integration or by applying the integration by parts method, written as follows:

$$\begin{aligned}
&\int_0^{l_c}\left(x_c-\frac{l_c}{2}\right)\frac{\mathrm{d}^4Y_c}{\mathrm{d}x_c^4}\mathrm{d}x_c=0,\ \int_0^{l_c}\left(x_c-\frac{l_c}{2}\right)\mathrm{d}x_c=0,\ \int_0^{l_c}\left(x_c-\frac{l_c}{2}\right)^2\mathrm{d}x_c=\frac{l_c^3}{12},\\
&\int_0^{l_c}\left(x_c-\frac{l_c}{2}\right)Y_c\mathrm{d}x_c=0,\int_0^{l_c}\left(x_c-\frac{l_c}{2}\right)\delta(x_c-l_{ci})\mathrm{d}x_c=l_{ci}-\frac{l_c}{2},\\
&\int_0^{l_c}\left(x_c-\frac{l_c}{2}\right)\delta(x_c-l_i)\mathrm{d}x_c=l_i-\frac{l_c}{2},\int_0^{l_c}\left(x_c-\frac{l_c}{2}\right)\frac{\mathrm{d}\delta(x_c-l_{ci})}{\mathrm{d}x_c}\mathrm{d}x_c=-1,\\
&\int_0^{l_c}\left(x_c-\frac{l_c}{2}\right)\frac{\mathrm{d}\delta(x_c-l_i)}{\mathrm{d}x_c}\mathrm{d}x_c=-1
\end{aligned}\tag{A11}$$

and

$$\begin{aligned}
&\int_0^{l}\left(x-\frac{l}{2}\right)\frac{\mathrm{d}^4Y}{\mathrm{d}x^4}\mathrm{d}x=0,\ \int_0^{l}\left(x-\frac{l}{2}\right)\mathrm{d}x=0,\ \int_0^{l}\left(x-\frac{l}{2}\right)^2\mathrm{d}x=\frac{l^3}{12},\ \int_0^{l}\left(x-\frac{l}{2}\right)Y\mathrm{d}x=0,\\
&\int_0^{l}\left(x-\frac{l}{2}\right)\delta(x-l)\mathrm{d}x=l-\frac{l}{2},\ \int_0^{l}\left(x-\frac{l}{2}\right)\delta(x)\mathrm{d}x=0-\frac{l}{2},\ \int_0^{l}\left(x-\frac{l}{2}\right)\frac{\mathrm{d}\delta(x-l)}{\mathrm{d}x}\mathrm{d}x=-1,\\
&\int_0^{l}\left(x-\frac{l}{2}\right)\frac{\mathrm{d}\delta(x)}{\mathrm{d}x}\mathrm{d}x=-1.
\end{aligned}\tag{A12}$$

Equations (A9) and (A10) become the following:

$$J_c\ddot{\theta}_c=\sum_{i=1}^{2}\left[F_{zci}\left(l_{ci}-\frac{l_c}{2}\right)+F_{zi}\left(l_i-\frac{l_c}{2}\right)\right]+\sum_{i=1}^{2}\left(M_i-hF_{xi}\right)\tag{A13}$$

$$J\ddot{\theta}=-(F_{z1}-F_{z2})\frac{l}{2}-(M_1+M_2)\tag{A14}$$

We now move on to the equations of the bending movement of the carbody and the anti-bending bars, respectively. For this, Equations (A1) and (A2) are multiplied by the eigenfunction of the first bending mode, $Y_c(x_c)$ of the carbody and $Y(x)$ of the anti-bending bars, and then integrated as follows:

$$\begin{aligned}
&E_cI_cT_c\int_0^{l_c}Y_c\frac{\mathrm{d}^4Y_c}{\mathrm{d}x_c^4}\mathrm{d}x_c+\mu_cI_c\dot{T}_c\int_0^{l_c}Y_c\frac{\mathrm{d}^4Y_c}{\mathrm{d}x_c^4}\mathrm{d}x_c+\rho_c\ddot{z}_c\int_0^{l_c}Y_c\mathrm{d}x_c+\rho_c\ddot{\theta}_c\int_0^{l_c}\left(x_c-\frac{l_c}{2}\right)Y_c\mathrm{d}x_c+\\
&\rho_c\ddot{T}_c\int_0^{l_c}Y_c^2\mathrm{d}x_c=\sum_{i=1}^{2}\left[F_{zci}\int_0^{l_c}Y_c\delta(x_c-l_{ci})\mathrm{d}x_c+F_{zi}\int_0^{l_c}Y_c\delta(x_c-l_i)\mathrm{d}x_c\right]-\\
&\sum_{i=1}^{2}\left[(M_i-hF_{xi})\int_0^{l_c}Y_c\frac{\mathrm{d}\delta(x_c-l_i)}{\mathrm{d}x_c}\mathrm{d}x_c\right],
\end{aligned}\tag{A15}$$

$$\begin{aligned}
&2\left[EIT\int_0^{l}Y\frac{\mathrm{d}^4Y}{\mathrm{d}x^4}\mathrm{d}x+\mu I\dot{T}\int_0^{l}Y\frac{\mathrm{d}^4Y}{\mathrm{d}x^4}\mathrm{d}x+\rho\ddot{z}\int_0^{l}Y\mathrm{d}x+\rho\ddot{\theta}\int_0^{l}\left(x-\frac{l}{2}\right)Y\mathrm{d}x+\rho\ddot{T}\int_0^{l}Y^2\mathrm{d}x\right]=\\
&-F_{zc1}\int_0^{l}Y\delta(x-l)\mathrm{d}x-F_{zc2}\int_0^{l}Y\delta(x)\mathrm{d}x+M_1\int_0^{l}Y\frac{\mathrm{d}\delta(x-l)}{\mathrm{d}x}\mathrm{d}x+M_2\int_0^{l}Y\frac{\mathrm{d}\delta(x)}{\mathrm{d}x}\mathrm{d}x.
\end{aligned}\tag{A16}$$

Then calculate the integrals as follows:

$$\begin{aligned}
&\int_0^{l_c}Y_c\frac{\mathrm{d}^4Y_c}{\mathrm{d}x_c^4}\mathrm{d}x_c=\int_0^{l_c}\left(\frac{\mathrm{d}^2Y_c}{\mathrm{d}x_c^2}\right)^2\mathrm{d}x_c,\ \int_0^{l_c}Y_c\mathrm{d}x_c=0,\ \int_0^{l_c}Y_c\left(x_c-\frac{l_c}{2}\right)\mathrm{d}x_c=0,\\
&\int_0^{l_c}Y_c\delta(x_c-l_{ci})\mathrm{d}x_c=Y_c(l_{ci}),\ \int_0^{l_c}Y_c\delta(x_c-l_i)\mathrm{d}x_c=Y_c(l_i),\\
&\int_0^{l_c}Y_c\frac{\mathrm{d}\delta(x_c-l_{ci})}{\mathrm{d}x_c}\mathrm{d}x_c=-\frac{\mathrm{d}Y_c(l_{ci})}{\mathrm{d}x_c},\ \int_0^{l_c}Y_c\frac{\mathrm{d}\delta(x_c-l_i)}{\mathrm{d}x_c}\mathrm{d}x_c=-\frac{\mathrm{d}Y_c(l_i)}{\mathrm{d}x_c},
\end{aligned}\tag{A17}$$

and

$$\int_0^l Y\frac{d^4Y}{dx^4}dx = \int_0^l \left(\frac{d^2Y}{dx^2}\right)^2 dx,\ \int_0^l Y dx = 0,\ \int_0^l Y\left(x-\frac{l}{2}\right)dx = 0,$$
$$\int_0^l Y\delta(x-l)dx = Y(l),\ \int_0^l Y\delta(x)dx = Y(0),\ \int_0^l Y\frac{d\delta(x-l)}{dx}dx = -\frac{dY(l)}{dx},\quad (A18)$$
$$\int_0^l Y\frac{d\delta(x)}{dx}dx = -\frac{dY(0)}{dx}.$$

Equations (A15) and (A16) become the following:

$$m_{mc}\ddot{T}_c + c_{mc}\dot{T}_c + k_{mc}T = \sum_{i=1}^{2}[F_{zci}Y_c(l_{ci}) + F_{zi}Y_c(l_i)] + \sum_{i=1}^{2}(M_i - hF_{xi})\frac{dY_c(l_i)}{dx_c} \quad (A19)$$

$$2m_m\ddot{T} + 2c_m\dot{T} + 2k_mT = -F_{z1}Y(l) - F_{z2}Y(0) + M_1\frac{dY(l)}{dx} + M_2\frac{dY(0)}{dx}, \quad (A20)$$

where m_{mc}, c_{mc}, and k_{mc} are the modal mass, damping, and stiffness for the FBM of the carbody (Equation (18)) and m_m, c_m, and k_m are the modal mass, damping, and stiffness associated to the first mode of the anti-bending bars (Equation (19)).

Inserting Equations (4) and (5) and the notations (20) in Equations (A5), (A6), (A13), (A14), (A19), and (A20), we obtain the resulting equations of motions (Equations (12)–(17)).

References

1. Chen, M.; Zhu, S.; Zhai, W.; Sun, Y.; Zhang, Q. Inversion and identification of vertical track irregularities considering the differential subgrade settlement based on fully convolutional encoder-decoder network. *Constr. Build. Mater.* **2023**, *367*, 130057. [CrossRef]
2. Sun, X.; Yang, F.; Li, S.; Zhang, Y.; Jing, G. Investigation of a dynamic chord method and its application on track irregularity evaluation and track maintenance. *Transp. Geotech.* **2023**, *38*, 100925. [CrossRef]
3. Mihailescu, I.M.; Popa, G.; Oprea, R. Detection of defects in the railway track that can influence traffic safety using the method of vibration analysis of vehicle-rail system. *Acta Tech. Napoc. Ser. -Appl. Math. Mech. Eng.* **2022**, *65*, 1241–1248.
4. Lee, C.-M.; Goderdovskiy, V.N.; Sim, C.-S.; Lee, J.-H. Ride comfort of a high-speed train through the structural upgrade of a bogie suspension. *J. Sound Vib.* **2016**, *361*, 99–107. [CrossRef]
5. Dumitriu, M. Ride comfort enhancement in railway vehicle by the reduction of the car body structural flexural vibration. *IOP Conf. Ser. Mater. Sci. Eng.* **2017**, *227*, 012042. [CrossRef]
6. Jing, L.; Wang, K.; Zhai, W. Impact vibration behavior of railway vehicles: A state-of-the-art overview. *Acta Mech. Sin.* **2021**, *37*, 1193–1221. [CrossRef]
7. Popa, G.; Andrei, M.; Tudor, E.; Vasile, I.; Ilie, G. Fast Detection of the Stick-Slip Phenomenon Associated with Wheel-to-Rail Sliding Using Acceleration Sensors: An Experimental Study. *Technologies* **2024**, *12*, 134. [CrossRef]
8. Arsene, S.; Sebesan, I.; Popa, G.; Gheti, M.A. Considerations on studying the loads on the motor bogie frame. *IOP Conf. Ser. -Mater. Sci. Eng.* **2018**, *400*, 042003. [CrossRef]
9. Cole, C.; Spiryagin, M.; Wu, Q.; Sun, Y.Q. Modelling simulation and applications of longitudinal train dynamics. *Veh. Syst. Dyn.* **2017**, *55*, 1498–1571. [CrossRef]
10. Liu, X.; Wang, P. Investigation of the generation mechanism of rail corrugation based on friction induced torsional vibration. *Wear* **2021**, *468*, 203593. [CrossRef]
11. Shu, Y.; Yang, G.; Liu, Z.; Dong, L. High-speed train axle fretting fatigue scaling experiment research and damage analysis. *Eng. Fail. Anal.* **2024**, *162*, 108317. [CrossRef]
12. Seo, J.-W.; Kwon, S.-J.; Lee, C.-W.; Lee, D.-H.; Goo, B.-C. Fatigue strength and residual stress evaluation of repair welding of bogie frame for railway vehicles. *Eng. Fail. Anal.* **2021**, *119*, 104980. [CrossRef]
13. Zhang, C.; Kordestani, H.; Shadabfar, M. A combined review of vibration control strategies for high-speed trains and railway infrastructures: Challenges and solutions. Journal of Low Frequency Noise. *Vib. Act. Control.* **2023**, *42*, 272–291.
14. Tomioka, T.; Takigami, T.; Suzuki, Y. Numerical analysis of three-dimensional flexural vibration of railway vehicle car body. *Veh. Syst. Dyn.* **2006**, *44*, 272–285. [CrossRef]
15. Miao, B.R.; Luo, Y.X.; Peng, Q.M.; Qiu, Y.Z.; Yang, Z.K. Multidisciplinary design optimization of lightweight carbody for fatigue assessment. *Mater. Des.* **2020**, *194*, 108910. [CrossRef]
16. Hui, C.; Weihua, Z.; Bingring, M. Vertical vibration analysis of the flexible carbody of high-speed train. *Int. J. Veh. Struct. Syst.* **2015**, *7*, 55–60. [CrossRef]

17. Yang, G.; Wang, C.; Xiang, F.; Xiao, S. Effect of train carbody's parameters on vertical bending stiffness performance. *Chin. J. Mech. Eng.* **2016**, *29*, 1120–1126. [CrossRef]
18. Diana, G.; Cheli, F.; Corradi, R.; Melzi, S. The development of a numerical model for railway vehicles comfort assessment through comparison with experimental measurements. *Veh. Syst. Dyn.* **2002**, *38*, 165–183. [CrossRef]
19. Morales, A.L.; Chicharro, J.M.; Palomares, E.; Ramiro, C.; Nieto, A.J.; Pintado, P. Experimental analysis of the influence of the passengers on flexural vibrations of railway vehicle carbodies. *Veh. Syst. Dyn.* **2021**, *60*, 2825–2844. [CrossRef]
20. Shi, H.L.; Wu, P. Flexible vibration analysis for car body of high-speed EMU. *J. Mech. Sci. Technol.* **2016**, *30*, 55–66. [CrossRef]
21. Palomares, E.; Morales, A.L.; Nieto, A.J.; Chicharro, J.M.; Pintado, P. Comfort improvement in railway vehicles via optimal control of adaptive pneumatic suspensions. *Veh. Syst. Dyn.* **2022**, *60*, 1702–1721. [CrossRef]
22. Lewis, T.D.; Jiang, J.Z.; Neild, S.A.; Gong, C.; Iwnicki, S.D. Using an inerter-based suspension to improve both passenger comfort and track wear in railway vehicles. *Veh. Syst. Dyn.* **2020**, *58*, 472–493. [CrossRef]
23. Sugahara, Y.; Kojima, T. Suppression of vertical vibration in railway vehicle carbodies through control of damping force in primary suspension: Presentation of results from running tests with meter-gauge car on a secondary line. *WIT Trans. Built Environ.* **2018**, *181*, 329–337.
24. Gong, D.; Wang, K.; Duan, Y.; Zhou, J. Car body floor vibration of high-speed railway vehicles and its reduction. *J. Low Freq. Noise Vibr. Act. Control* **2020**, *39*, 925–938. [CrossRef]
25. Dumitriu, M. Study on improving the ride comfort in railway vehicles using anti-bending dampers. *Appl. Mech. Mater.* **2018**, *880*, 207–212. [CrossRef]
26. Graa, M. Modeling and control for vertical rail vehicle dynamic vibration with comfort evaluation. *Int. J. Math. Model. Methods Appl. Sci.* **2017**, *11*, 240–245.
27. Gong, D.; Zhou, J.; Sun, W. Passive control of railway vehicle car body flexural vibration by means of under frame dampers. *J. Mech. Sci. Technol.* **2017**, *31*, 555–564. [CrossRef]
28. Nitish, A.; Singh, K. Active control of railway vehicle suspension using PID controller with pole placement technique. *Mater. Today Proc.* **2023**, *80*, 278–284. [CrossRef]
29. Kozek, M.; Benatzky, C.; Schirrer, A.; Stribersky, A. Vibration damping of a flexible car body structure using piezo-stack actuators. *IFAC Proc. Vol.* **2008**, *4*, 8287–8292. [CrossRef]
30. Kamada, T.; Hiraizumi, T.; Nagai, M. Active vibration suppression of lightweight railway vehicle body by combined use of piezoelectric actuators and linear actuators. *Veh. Syst. Dyn.* **2010**, *48*, 73–87. [CrossRef]
31. Sharma, S.K.; Sharma, R.C.; Lee, J.; Jang, H.L. Numerical and experimental analysis of DVA on the flexible-rigid rail vehicle carbody resonant vibration. *Sensors* **2022**, *22*, 1922. [CrossRef] [PubMed]
32. Huang, C.; Zeng, J.; Luo, G.; Shi, H. Numerical and experimental studies on the car body flexible vibration reduction due to the effect of car body-mounted equipment. *Proc. Inst. Mech. Eng. Part F J. Rail Rapid Transit* **2016**, *232*, 103–120. [CrossRef]
33. Gong, D.; Zhou, J.S.; Sun, W.J. On the resonant vibration of a flexible railway car body and its suppression with a dynamic vibration absorber. *J. Vib. Control* **2013**, *19*, 649–657. [CrossRef]
34. Dumitriu, M. A new passive approach to reducing the carbody vertical bending vibration of railway vehicles. *Veh. Syst. Dyn.* **2017**, *55*, 1787–1806. [CrossRef]
35. Dumitriu, M.; Mazilu, T.; Apostol, I.I. Scale Models to Verify the Effectiveness of the Methods to Reducing the Vertical Bending Vibration of the Railway Vehicles Carbody: Applications and Design Elements. *Appl. Sci.* **2023**, *13*, 2368. [CrossRef]
36. Mazilu, T.; Dumitriu, M.; Sorohan, Ș.; Gheți, M.A.; Apostol, I.I. Testing the Effectiveness of the Anti-Bending Bar System to Reduce the Vertical Bending Vibrations of the Railway Vehicle Carbody Using an Experimental Scale Demonstrator. *Appl. Sci.* **2024**, *14*, 4687. [CrossRef]
37. Cheli, F.; Corradi, R. On rail vehicle vibrations induced by track unevenness: Analysis of the excitation mechanism. *J. Sound Vib.* **2011**, *330*, 3744–3765. [CrossRef]